Computers & Geosciences 102 (2017) 22–33

Contents lists available at ScienceDirect

Computers & Geosciences

journal homepage: www.elsevier.com/locate/cageo

Research paper

Unsupervised detection of topographic highs with arbitrary basal shapes based on volume evolution of isocontours

Costas Panagiotakis[a,c,*], Eleni Kokinou[b,c]

[a] Department of Business Administration, Technological Educational Institute of Crete, 72100 Agios Nikolaos, Crete, Greece
[b] Department of Environmental and Natural Resources Engineering, Technological Educational Institute of Crete, 3 Romanou, Halepa, 73133 Chania, Greece
[c] Foundation for Research and Technology-Hellas, Institute of Computer Science, 70013 Heraklion, Crete, Greece

ARTICLE INFO

Keywords:
Digital Elevation Model
Topographic high
Isocontour
Geomorphological features

ABSTRACT

In this work, an unsupervised isocontour based segmentation method is proposed, that is applied on the detection of topographic highs with arbitrary basal shapes on Digital Elevation Models (DEMs). A series of isocontour based segmentation maps is computed for decreasing altitude levels. During this process, the isocontours are gradually merged providing a topological hierarchy of highs in an inclusion tree structure. A novel formulation of a topographic high is given taking into account the volume evolution of an isocontour that starts from the top of a high and grows, as decreasing the altitude level of isocontour, until a high of higher altitude is reached. This formulation yields to a robust unsupervised algorithm that can be sequentially applied to automatically recognize and discriminate the topographic highs of a region according to the inclusion tree without any constraint on basal shapes. The proposed method is applied on real and synthetic DEMs, in order to automatically detect the exact shape of complex topographic highs and some geomorphological based features useful for high annotations, yielding high performance results, even if the highs are partially visible in the given DEM.

1. Introduction

The automatic extraction of geomorphic features (Kweon and Kanade, 1994) constitutes a rapid growing technology, widely used in the interpretation of high resolution Digital Elevation Model (DEMs). In recent years, the techniques of the automatic identification are sufficiently stabilized, increasing the accuracy and reliability of the interpreted features. In Podobnikar (2012), peak detection and shape delineation is solved based on image-processing and spatial-analysis techniques (e.g., developing inventive variables using an annular moving window) under high quality DEMs. This work has some similarities with the proposed method, since it also uses local peaks as a local maximum in elevation as well as the isocontours (e.g. by the relative elevation) to determine the peak shape features. Additionally, isocontours were used by Obu and Podobnikar (2013) on the inverse problem of high detection called karst depression.

In our previous work (Panagiotakis and Kokinou, 2014), a method concerning the enhancement and identification of the geological faults in the sea, has been proposed. According to this method, the Slope and Aspect images as well as their derivatives are computed and efficiently combined with a rotation and scale invariant filter and a pixel labelling method, providing an enhancement of the sea faults and the detection of points that may belong to them. In Panagiotakis and Kokinou (2015), we extend the aforementioned method in onshore and offshore environment by taking into account the topology of the geological faults and adding constraints on the fault shape, in order to detect the linear patterns of the faults. Inspired by Panagiotakis and Kokinou (2014, 2015), in the current paper we further continue the analysis of DEMs.

So, in this work, we study the problem of the automatic unsupervised detection of topographic highs using digital elevation models (DEMs). DEMs constitute a valuable source of information in a variety of geoscientific disciplines, in order to recognize the surface features. Topographic maps, aerial-satellite images and airborne-terrestrial laser scanners are among the most important data sources, used in the last years in high resolution topographic surveys to further improve the terrain analysis (Tarolli et al., 2009; Slatton et al., 2007). For example, high resolution topography is efficiently used in the recognition of surface lineaments possibly related to faulting (Panagiotakis and Kokinou, 2015), in the mapping of glacial landforms (Smith et al., 2006), in the characterization of depositional features (Frankel and Dolan, 2007), in the evaluation of landslide activity (Booth et al., 2009), in the characterization of channel bed morphology (Cavalli and

* Corresponding author at: Department of Business Administration, Technological Educational Institute of Crete, 72100 Agios Nikolaos, Crete, Greece.
E-mail addresses: cpanag@staff.teicrete.gr (C. Panagiotakis), ekokinou@staff.teicrete.gr (E. Kokinou).

http://dx.doi.org/10.1016/j.cageo.2017.02.004
Received 22 September 2016; Accepted 3 February 2017
Available online 04 February 2017
0098-3004/

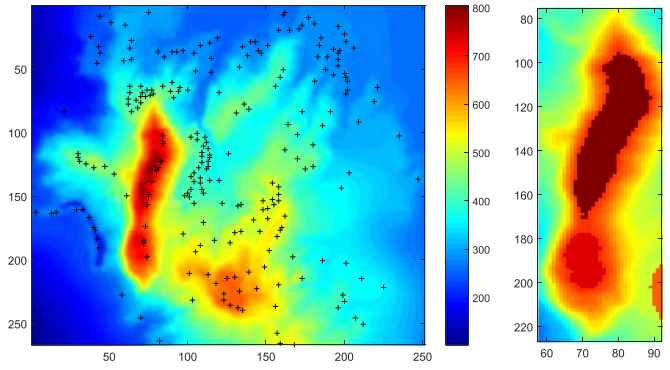

Fig. 1. (a) The DEM of Giouchtas region. The tops are depicted with black plus sign. (b) The detected highs of the proposed method in the main mountainous region of Giouchtas. A reference grid has been selecting for indexing.

Marchi, 2008), in geo-archaeology (Davis, 2012) and many other applications.

The proposed method of topographic high detection is based on the volume expansion of isocontours, which provides a series of isocontour based segmentation maps for decreasing altitude levels. It holds that the more challenging problem is the detection and discrimination of the topographic highs with complex shape that are close together. An example of a complex DEM is given in Fig. 1(a) corresponding to an environmentally protected area located in central Crete (Greece). The elevation in this region is ranging between 102 m and 803 m with an average altitude of 352 m. In this figure, the 232 tops, detected in the region, are plotted using the black plus (+) symbol. The detection of the topographic highs constitutes a quite difficult task, because.

- several tops are close together and
- some isocontours reveal quite complex shapes.

So, it is not clear how many highs have to be detected even in the well discriminated central part of Giouchtas Mountain (see left part of Fig. 1(a)), where the topographic point with the highest altitude is located. In this work, we provide a formal definition of high proposing a methodology to compute the topographic highs, by detecting an area associated with a local maximum (i.e. mountain) (see Section 3). Fig. 1(b) depicts the result of the proposed method that successfully detect two highs in Giouchtas Mountain. The two detected highs are depicted with colors corresponding to the altitude of their tops (803 m and 736 m).

Image segmentation methods (Panagiotakis et al., 2011) group the image pixels into non overlapping segments, so if we apply them to solve the high detection problem we need an extra step to automatically recognize the highs. Additionally, the application of most image segmentation methods on highs detection mainly fail due to the fact that there does not exist any clear boundary to determine highs. The region growing algorithm, proposed in Panagiotakis et al. (2011), has some similarities with the proposed method. It propagates initially labelled regions (contours) towards the space of unlabelled image pixels, where the initially labelled pixels are defined to be at the zero level in the topographic map interpretation of a classification criterion. In this work, isocontours are also propagated starting from local peaks.

In Kweon and Kanade (1994), a methodology is presented for building high level terrain descriptions, referred to as topographic maps, by extracting terrain features like “peaks”,“pits”,“ridges”, and “ravines” from the contour map. Similarly with Kweon and Kanade (1994), in the present work the topographic features are defined based on isocontours and a tree-like structure (inclusion tree), that is a hierarchical representation of the enclosure relationships among the isocontours. Additionally, the method proposed in Hong and Sohn (2010) has some similarities to our work. The goal of this work is to

Table 1
Symbol table.

Symbols	Definitions
I	Given DEM
ν, u	Two tops (local maxima) of I
r	An altitude level of I
$c_\nu(r)$	Isocontour of top ν and altitude level r
$R_\nu(r)$	The region enclosed by the isocontour $c_\nu(r)$
$\|R_\nu(r)\|$	The area of the region $R_\nu(r)$
$V_\nu(r)$	The volume of region $R_\nu(r)$ as r decreases
$\dot{V}_\nu(r)$	The volume derivative of region $R_\nu(r)$ as r decreases
$NVD_\nu(r)$	The normalized volume derivative

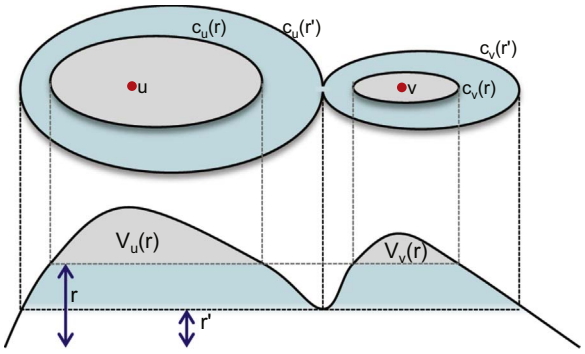

Fig. 3. Schematic illustration of two isocontours' evolution.

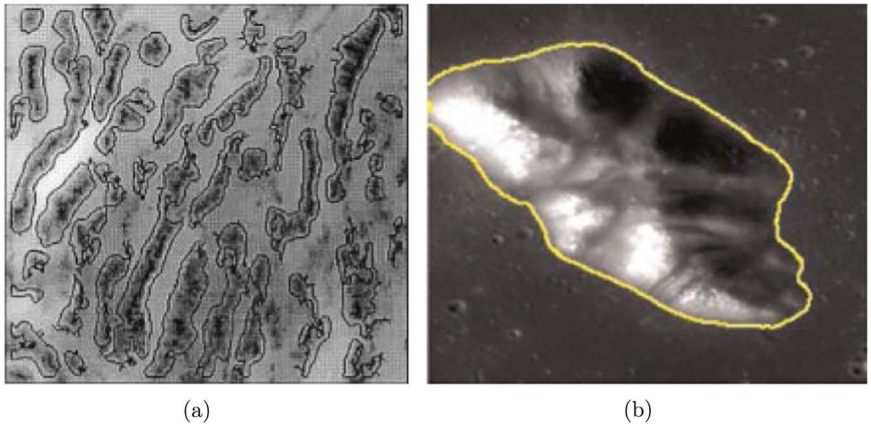

Fig. 2. The mountain detection results according to (a) (Miliaresis and Argialas, 1999) and (b) (Micheal and Vani, 2015) methods.

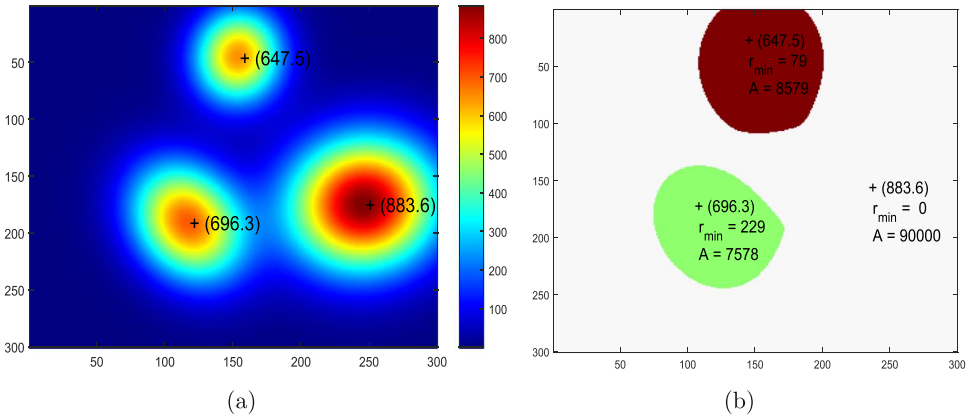

Fig. 4. (a) A synthetic DEM of three tops. (b) The maximum expanded region $R_v(r_{min})$ for the three tops of the synthetic DEM of (a). For each top, r_{min} and the corresponding area are also plotted. A reference grid has been selecting for indexing the two images. In each detected topographic high the maximum altitude (m) the r_{mim} (m) and the area (m^2) are provided.

detect and segment salient regions in mammograms. A topographic representation has been developed using isocontours like in our framework. In a similar way with the present work, the topological and geometrical structure of the image is analyzed using an inclusion tree (Kweon and Kanade, 1994; Hong and Sohn, 2010). The detected isocontours correspond to the boundaries of distinctive regions with abrupt intensity changes retaining the same topology. The final detection of breast boundary and the pectoral muscle is done using anatomical information of the saliency of contours.

2. Material and methods

The automatic segmentation and classification of DEMs into several classes has been well studied in literature. Iwahashi and Pike (2007) proposed an iterative procedure that automatically divides a DEM into categories of surface form based on three local features i.e. the slope gradient, the local convexity, and the surface texture. The classification step combines twofold-partitioned maps of the three variables converted to greyscale images, using the mean of each variable as the dividing threshold. Similarly, in Drăguţ and Blaschke (2006), the elevation, the profile curvature, the plan curvature and the slope gradient are computed. Next, the homogenous regions are computed at several levels through image segmentation. The classification, defined using flexible fuzzy membership functions, has nine classes: peaks and toe slopes (defined by the altitudinal position or the degree of dominance), steep slopes and flat/gentle slopes (defined by slope gradients), shoulders and negative contacts (defined by profile curvatures), head slopes, side slopes and nose slopes (defined by plan curvatures).

In literature, several works have been proposed to solve the mountain detection problem from DEM. Miliaresis and Argialas (1999) developed a methodology to classify the Global Digital Elevation Model(GTOPO30) into three terrain classes (mountains, basins and piedmont slopes). Seeds ridge, valley cells and selected gradient-region growing criteria are taken into account in a region-growing segmentation algorithm in order to extract the mountains and the basins. In Dinesh (2006), a mathematical morphological based algorithm to perform the extraction of mountains from DEM has been proposed. First, ultimate erosion is used to extract the peaks of the DEM. Finally, conditional dilation is performed on the extracted peaks to obtain the mountain regions. Micheal and Vani (2015) proposed an approach for mountain detection from lunar DEM. It consists of several steps like denoising, extracting texture information, choosing an appropriate threshold using the Renyi Entropy method, then the post-processing (edge detection) to extract the boundary of the mountain. Bohnenstiehl et al. (2012) presented an approach, called

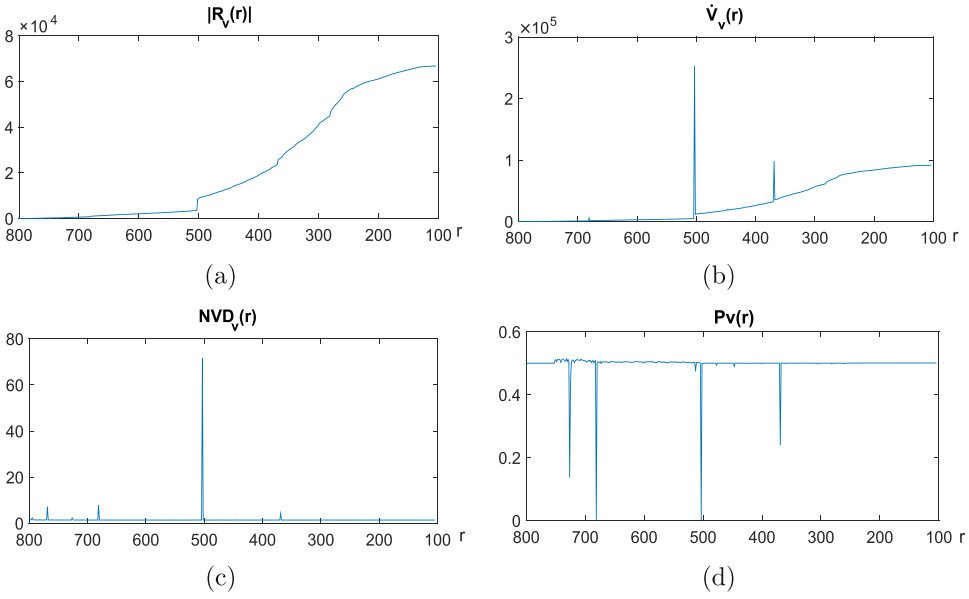

Fig. 5. (a) $|R_v(r)|$, (b) $\dot{V}_v(r)$, (c) $NVD_v(r)$ (d) $P_v(r)$ corresponding to the highest top in the real data of Fig. 1(a).

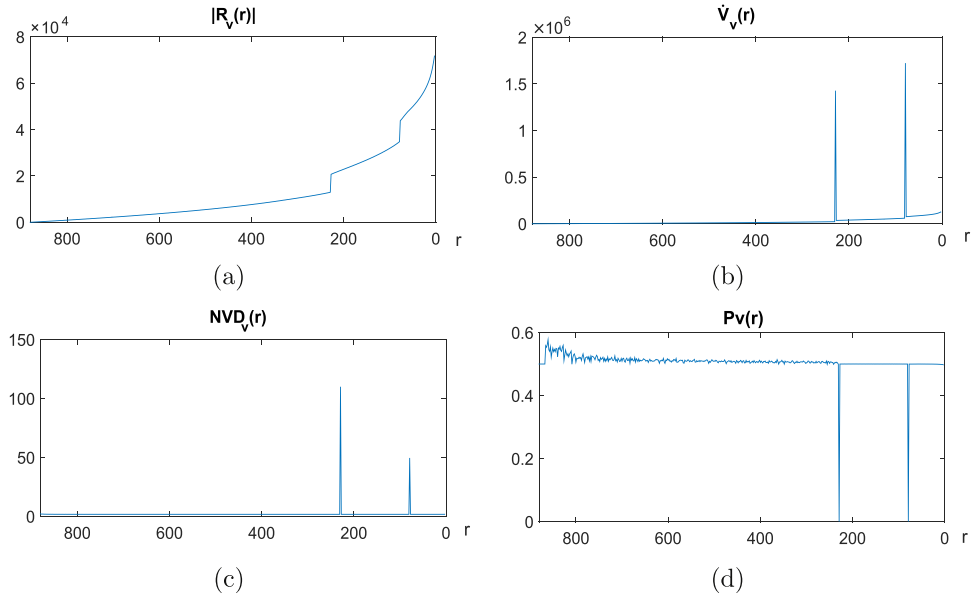

Fig. 6. (a) $|R_v(r)|$, (b) $V_v(r)$, (c) $NVD_v(r)$ and (d) $P_v(r)$ corresponding to the highest top (883.6 m) in the synthetic data of Fig. 4(a).

Fig. 7. Scheme of the main steps of the proposed system.

MBOA, for identification and characterization of topographic highs having quasi-elliptical basal shapes designed for the study of volcanic edifices in sub-aerial and sub-marine environments. Even if it is designed for the study of volcanic edifices, it can be applied to identify any enclosed topography feature within a DEM. Initially, MBOA utilizes the results of a standard closed- contouring approach, and then adjusts the elevation of the volcanic base by evaluating the shape of the edifice along a series of topographic profiles. In our experimental results, the proposed method is compared with MBOA. NETVOLC (Euillades et al., 2013) is another recent algorithm for automatically computing the boundary of volcanic edifices. It applies minimum cost flow (MCF) networks for computing the best possible edifice outline using a DEM and its first-and second-order derivatives.

Most of the aforementioned methods work well when the topographic highs are well separated with distinct boundaries, mostly related to steep slopes. They detect sudden changes on slopes and curvatures to determine the boundaries of the mountain without optimizing any global criterion. Fig. 2 presents mountain detection results according to Miliaresis and Argialas (1999) and Micheal and Vani (2015) methods. According to the results of Fig. 2, it holds that both methods well recognize the mountain structures, but they yield under-segmented results concerning the high detection problem, since they are not able to discriminate highs that belong on complex mountain structures and are close together merging them into one region. In Fig. 2(a) some closed highs are merged into the same detected group, while in Fig. 2(b) the detected region can be divided into several highs. The method proposed in Bohnenstiehl et al. (2012) works under the assumptions that the topographic highs have quasi-elliptical basal shapes. On the contrary, the proposed method has been designed to solve this problem without any assumption on the number and shape of highs. The highs' separation can be also used to enforce the detection of geological faults (Panagiotakis and Kokinou, 2015) both in direction and location, related to topographic highs and to confirm the results of the automatic detection with field measurements, as shown later in this work in the example concerning the geomorphological features of the Giouchtas region. At the same time, the methods from literature ignore the necessary constraint that a high boundary should be an isocontour like the proposed method does. The proposed method is able to detect highs of complex basal shapes even if they are partially visible in the given DEM.

Additionally, according to our knowledge the current work faces for the first time the problem of the formal definition of a topographic high based on volume evolution of isocontours. This formulation yields to a robust unsupervised algorithm that is sequentially applied to automatically recognize the topographic highs of a region. The highs' boundaries are given as solutions of a probability optimization problem based on the volume evolution of an isocontour starting from the top and gradually growing, as decreasing the altitude level of the isocontour. The proposed framework has been tested and compared with Bohnenstiehl et al. (2012) on real and synthetic topographic data, where highs of various orientation, density and size are presented, yielding high performance results.

The rest of the paper is organized as follows: Sections 3 and 4 describe the problem formulation and the proposed methodology for the high detection, respectively. The experimental results are presented and discussed in Section 5. Finally, conclusion is provided in Section 6.

3. Problem formulation

In this section, we set the scene of the various aspects of the problem that this paper addresses, and concurrently we present the stepping-stones where our subsequent developments are based on. Table 1 summarizes the symbols' definitions used in this work. The input of the proposed method is a DEM I (e.g. see Figs. 1(a), 4(a)). Hereafter, several notations and definitions are given related to the problem of topographic high detection:

- Let $\nu \in I$ be a top (local maxima) of a DEM I.
- Let $R_\nu(r)$ be the region enclosed by the isocontour $c_\nu(r)$, with $\nu \sqsubset c_\nu(r)$, where $\sqsubset$denotes the spatial enclosure relationship, i.e., the point (top) ν is spatially enclosed by the contour $c_\nu(r)$.
- Let $V_\nu(r)$ be the volume of the 3D surface enclosed by the $R_\nu(r)$ and the DEM I.
- r denotes the altitude level of an isocontour, where $r \in [r_{min}, I(\nu)]$.
- r_{min} is the minimum value of r so that $I(\nu) \geq I(p)$, $\forall\, p \in R_\nu(r)$. Therefore, the maximum expanded region for the high correspond-

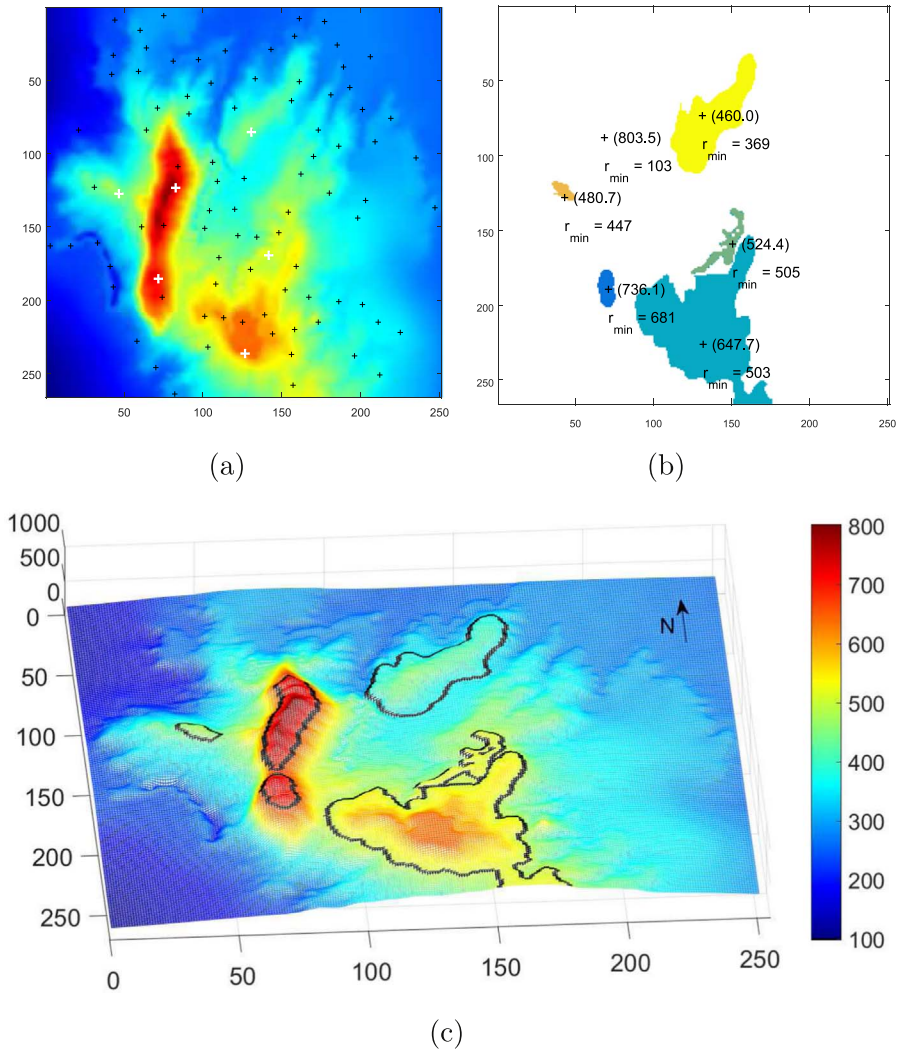

Fig. 8. (a) The result of the subsampling step and the *FS* set (white plus). (b) The maximum expanded region $R_\nu(r_{min})$ for the six tops of the *FS* set. The maximum altitude (in m) and the r_{min} (m) are also provided for each detected topographic high, shown in different color. (c) The final results of the VOLEI method projected on Giouchtas DEM. The vertical scale corresponds to the elevation (m) of the study area.

ing to the top v is $R_\nu(r_{min})$.

- The topological relationship of isocontours, as r decreases, can be represented by a tree structure, called the inclusion tree.

Fig. 3 depicts a schematic illustration of two isocontours evolution. The isocontours $c_\nu(r)$ and $c_u(r)$ and the corresponding volumes $V_\nu(r)$ and $V_u(r)$ are depicted in gray color. The altitude level r' is the r_{min} of top v, and the $R_\nu(r_{min})$ is enclosed by the $c_\nu(r')$. Concerning the top u, it holds that $r_{min} = 0$, since $I(u) > I(\nu)$. The inclusion tree of this example has two levels and two nodes, the root (top u) and its leaf (top v).

3.1. Topographic high properties

A topographic high has the following properties that are used in its formal definition. As the altitude level r decreases, the area $|R_\nu(r)|$ and its volume $V_\nu(r)$, that correspond to $c_\nu(r)$ (isocontour of the top v with altitude level r), increase. Additionally, it holds that when the given $c_\nu(r)$ is smoothly expanded as r decreases, the first derivative of volume with respect to r (volume derivative),

$$\dot{V}_\nu(r) = \frac{dV_\nu(r)}{dr} \tag{1}$$

linearly increases, due to the fact that the area $|R_\nu(r)|$ quadratically increases. The Normalized Volume Derivative $NVD_\nu(r)$ by the area $(|R_\nu(r)|)$ is used to detect the topographic highs, since it is almost stable when the isocontour $c_\nu(r)$ is smoothly expanded.

$$NVD_\nu(r) = \frac{\dot{V}_\nu(r)}{|R_\nu(r)|} \tag{2}$$

Rapid and unpredictable changes of $NVD_\nu(r)$ are used to discriminate regions that belong to different topographic highs.

3.2. Definition of a topographic high

The problem of topographic high detection, that we tackle in this research, is defined as follows: The high's region (of optimal r) $R_\nu(r_{opt})$ with $R_\nu(r_{opt}) \subseteq R_\nu(r_{min})$ of a top ($\nu \in I$) is defined by the cells enclosed by a suitable isocontour $c_\nu(r_{opt})$ so that

$$r_{opt} = \text{argmin}_r Pr(X > NVD_\nu(r)),\ r \in [r_{min}(\nu), I(\nu)] \tag{3}$$

$Pr(X > NVD_\nu(r))$ is the probability of the random variable X to be higher than the normalized volume derivative of top ν and altitude level r. To simplify the notations, hereafter we use $P_\nu(r)$ instead of $Pr(X > NVD_\nu(r))$.

In Fig. 3, concerning the top u it holds that $r_{opt} = r'$, since $NVD_u(r') \gg NVD_u(r)$, $r > r'$. According to this definition, the problem of high detection is reduced to the problem of selecting the suitable

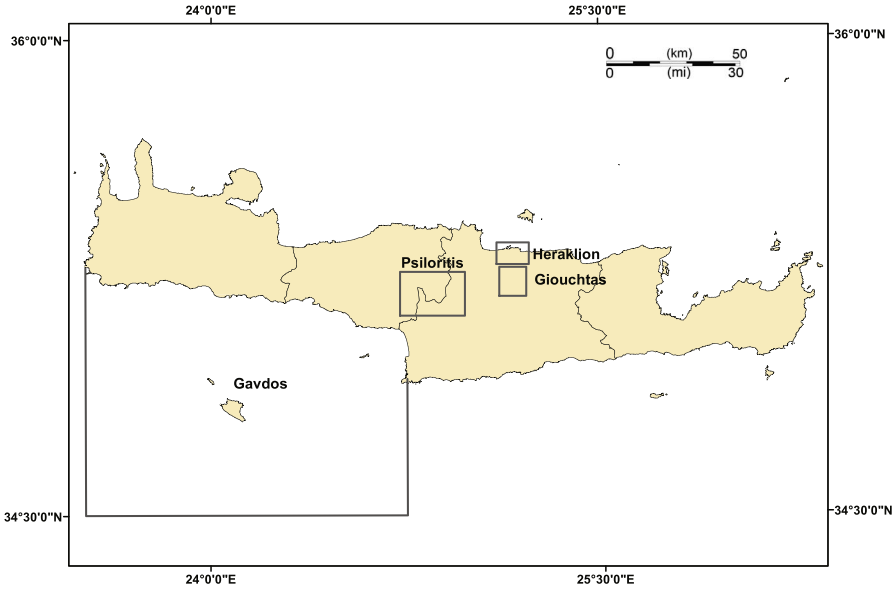

Fig. 9. The global map of locations of particular study areas.

isocontour, where the probability of the volume derivative value is minimized and can not be described by the current distribution of volume velocities (e.g. due to tops merging).

In Fig. 4(a), a DEM of three synthetic topographic highs of almost ellipsoid shape is shown. The three tops of highs are depicted with plus symbols, having altitudes 883.6 m, 696.3 m and 647.5 m respectively. Fig. 4(b) depicts with different colors the maximum expanded regions $R_\nu(r_{min})$ for the three tops of the synthetic DEM of Fig. 4(a). The top's altitude is also given in parenthesis. The region corresponding to the highest top can be expanded on the entire image. For each top, r_{min} and the corresponding area (A) are also plotted. It holds, that the maximum expanded area of the third top is higher than the maximum expanded area of the second top due to their relative positions. The inclusion tree of this example has two levels and three nodes, the root (highest top) and two leaves (the two other tops).

Figs. 5 and 6 depict the $|R_\nu(r)|$, $\dot{V}_\nu(r)$, $NVD_\nu(r)$ and $P_\nu(r)$ for the two tops presenting the highest altitudes of Fig. 1(a) and 4(a), respectively. In both cases, as the altitude level r decreases the $|R_\nu(r)|$ and the $\dot{V}_\nu(r)$ increase, while the normalized volume derivative $NVD_\nu(r)$ and the $P_\nu(r)$ are almost stable appearing rapid changes on altitude levels that correspond to regions' merging. In the example corresponding to the real data (see Fig. 5), rapid changes are present in some altitude levels due to the high number of tops. Concerning the example of the synthetic data (see Fig. 6), two distinct rapid changes are indicated in the graphs of $NVD_\nu(r)$ and $P_\nu(r)$, corresponding to the merging of the second and third tops' regions, with the highest one.

3.3. Geomorphological features

In this section we define several geomorphological features based on the proposed high detection method that can be used to annotate the detected high. The following global geomorphological features are computed based on the isocontour $c_\nu(r_{opt})$ of the detected high of top v. Isocontours have been also used in Kweon and Kanade (1994) to define high level local terrain descriptions.

- **Orientation**: It is given by the angle between the horizontal axis and the major axis of the ellipse that has the same second order moments (Panagiotakis et al., 2008) as the detected high region. The orientation of zero or 180° angle is parallel on horizontal plane. Usually, it holds that the main orientations of nearby highs are similar that checks the quality of the automatic shape detection.
- **Eccentricity**: It is defined by the ratio of the distance between the foci of the ellipse that has the same second order moments as the detected high region and its major axis length. Its' value is between zero (for circle) and one (for line).
- **Average Slope**: It is given by the basis angle of the cone that has the same relative elevation of the high and circular basis area equal to $|R_\nu(r_{opt})|$. The relative elevation is given by the difference between the elevation of the top $I(\nu)$ and the elevation of the isocontour $c_\nu(r_{opt})$, r_{opt}. This metric is not affected by local shape variations. The average slope is measured in the range of 0–90°.
- **Shape Complexity**: It is given by the ratio of the high area divided by the area of the cone that has the same relative elevation of the high and circular basis area equal to $|R_\nu(r_{opt})|$. In both areas, we don't take into account the bases of the 3D shapes. This metric is correlated with the variance of local slope and it increases as shape complexity (local surfaces variations) increases.

4. Methodology

The problem of high detection, that we tackle in this research, is described hereafter. The input of the proposed method is a DEM I. Taking into account the hierarchy of the tops in the inclusion tree, the proposed method, called VOLEI, is able to automatically detect the highs based on the VOlume EVolution of an Isocontour (VOLEI). The pseudo-code of the proposed method (VOLEI) is depicted in Algorithm 1. The proposed method can be divided into the following steps that are also depicted in Fig. 7:

- Initially, the local maxima (tops) of the DEM are computed. In order to ignore highs corresponding to very low areas, the parameter $MinA$ is used to define the minimum possible expanded area of a high. Therefore, for each detected high holds $|R_\nu(r_{opt})| \geq MinA$. The parameter $MinA$ is also used to sample the tops, that are very close together, in order to reduce the computational cost without affecting the method's performance. A top is selected if and only if it is the highest top in its neighbourhood, that is defined by the block of size $\sqrt{MinA} \times \sqrt{MinA}$. Let ST be the set of selected tops (see lines 1–7 of Algorithm 1). Fig. 8(a) depicts the result of subsampling. In this example, we get only 92 tops (plus sign) from the 232 tops of Fig. 1(a) using $MinA$=100 pixels (cells).

- Next, the sequence of isocontours for different decreasing levels r are computed and the evolution of the area as well as the normalized volume derivative (see Eq. (2)) are computed for each top of ST. In this work, we have used 512 different equidistant levels r between the highest and the lowest altitudes of the entire image. The tops with $|R_v(r_{min})| < MinA$ are also removed from ST set, yielding the final tops set (FT), lines 8–14 of Algorithm 1. Fig. 8(a) depicts the result of this step, where only six tops (white plus sign) from 92 tops are finally included in the FT set. Fig. 8(b) illustrates the maximum expanded region $R_v(r_{min})$ for the six tops of the FT set. The $R_v(r_{min})$ of the highest top (803 m) corresponds to the entire image. The altitude of tops is also provided in parenthesis.
- Finally, for each top v of the FT set, according to the hierarchy of the inclusion tree (starting from the highest top - see line 15 of Algorithm 1)) we apply the equations presented in Section 3 to compute $P_v(r)$. The high corresponding to a top v is detected, only if $\min_r P_v(r) < 5\%$ (defined by trial and error), otherwise it is ignored (see lines 17–26 of Algorithm 1). Additionally, in order to get non overlapping segments (highs), when a high $R_v(r_{opt})$ is detected, we remove from the FT set the tops u that are enclosed by the isocontour $c_v(r_{opt})$ (see lines 19–23 of Algorithm 1). Due to the hierarchy of the inclusion tree, it holds that the altitude of those tops u is lower than the altitude of v. Fig. 8(c) depicts the final result of the VOLEI method projected on Giouchtas DEM, where six highs have been detected. The isocontours (boundaries) of the detected highs are plotted with black curves.

Algorithm 1. The pseudocode of the VOLEI algorithm.

input: I, $MinA$.
output: FT and $c_v(r_{opt})$, $v \in FT$

1 $ST = \emptyset$
2 **foreach** $p \in I$ **do**
3 $x = \text{argmax}_y\{I(y), 0 < |y - p|_1 < \frac{\sqrt{MinA}}{2}\}$
4 **if** $I(p) \geq I(x)$ *and* $\min_{v \in ST}|v - z|_1 > \frac{\sqrt{MinA}}{2}$ **then**
5 $ST = ST \cup \{p\}$
6 **end**
7 **end**
8 $FT = \emptyset$
9 **foreach** $v \in ST$ **do**
10 $[R_v, P_v, c_v(r_{opt})] = getIsoCurves(I, v)$
11 **if** $|R_v(r_{min})| \geq MinA$ **then**
12 $FT = FT \cup \{v\}$
13 **end**
14 **end**
15 $FT = sortInDescentedOrder(FT, I)$
16 **foreach** $v \in FT$ **do**
17 **if** $\min_r P_v(r) < 5\%$ **then**
18 $FT = FT \cup \{v\}$
19 **foreach** $u \in FT$ **do**
20 **if** $u \sqsubset c_v(r_{opt})$ **then**
21 $FT = FT - \{u\}$
22 **end**
23 **end**
24 **else**
25 $FT = FT - \{v\}$
26 **end**
27 **end**

Results and discussion

The VOLEI method has been evaluated using elevation and bathymetric metadata. Bathymetry has been obtained from the European Marine Observatory and Data Network (EMODNet) Hydrography portal.[1] Elevation data are from the topographic maps of a scale 1:50,000 and 1:5,000, respectively, published by the Hellenic Army Geographical Service (H.A.G.S).

In this work, we used real data (Fig. 9) under different spatial resolutions that correspond to three selected regions from Crete (Greece) presenting different morphological characteristics, a bathymetric image that corresponds to Gavdos region (offshore South Crete) and finally we applied the proposed method on the DEM of Crete island. Fig. 9 depicts the locations of the particular study areas. So, the four locations that are used in this work include:

- Giouchtas region with a spatial resolution of 30 m
- Heraklion region with a spatial resolution of 34 m
- Psiloritis Mountain with a spatial resolution of 50 m
- Gavdos region with a spatial resolution of 300 m
- Crete island with a spatial resolution of 50 m

5.1. Experimental results and comparisons

In this section, the experimental results of the proposed framework and comparisons with MBOA method (Bohnenstiehl et al., 2012) are presented. Fig. 10 depicts the results of MBOA (first column) and the VOLEI method (second column) under different real elevation and bathymetric images. The DEMs correspond to selected regions from Crete (Greece), showing both rough and smooth topography, i.e. Giouchtas region (Central Crete Figs. 10(a) and (b)), Heraklion region (Figs. 10(c) and (d)) and Psiloritis Mountain (Fig. 10(e) and (f)) with maximum altitudes 803 m, 298 m and 2440 m, respectively. In Figs. 10(g) and (h), the bathymetric image corresponds to Gavdos region (offshore South Crete) with maximum depth 3628 m. In the first column of Fig. 10, the initial isocontours of the detected highs are plotted with white curves and the final detections according to the MBOA method are plotted with black curves. In the second column of Fig. 10, the isocontours (boundaries) of the detected highs, according to the VOLEI method, are plotted with black curves and the altitudes of the tops (black plus sign) are also given in parenthesis. In Fig. 10(b), (d), (f) and (h) six, ten, eleven and eight highs have been detected, respectively. Under any case, the proposed method successfully detects the complex shape of highs even in case they are close together (see Fig. 10(b)) or partially visible (see Fig. 10(d)). On the contrary MBOA method fails to discriminate some complex shape of highs (see Fig. 10(c)) and highs that are close together (see Fig. 10(a)).

Fig. 11 depicts the results of the proposed method under Crete DEM (1:50.000). We applied the proposed algorithm on the DEM of the entire island of Crete in order to check its efficiency in larger areas and smaller scale topographic data. The results of the proposed methodology (Fig. 11) are quite satisfactory. In this example, 303 highs in Crete are detected. The topographic highs of the three major mountains (i.e the White Mountains or Lefka Ori (2452 m), the Idi Range (2456 m) and the Dikti Mountains (2148 m)) are automatically detected with great accuracy in location and shape. Additionally, highs, belonging to the rest mainland having lower elevations are also successfully detected.

Additionally, for the purpose of this research a synthetic dataset has been created, consisting of 180 DEMs (300×300 grid cells). Each DEM $I_{k,j}$ of the synthetic dataset is given by the sum of k, $k \in \{2, \ldots, 10\}$ 2D Gaussian functions $G_{k,j}$, of random orientation θ, altitude ($H \in [500, 1000]$), center (x_0, y_0) and spreads ($\sigma_x, \sigma_y \in [5\%, 10\%]$ of image diagonal), as defined in Eq. (4). For each number k, we have created 20 DEMs ($j \in \{1, \ldots, 20\}$). So, the synthetic dataset consists of $9 \times 20 = 180$ DEMs.

[1] http://www.emodnet-hydrography.eu

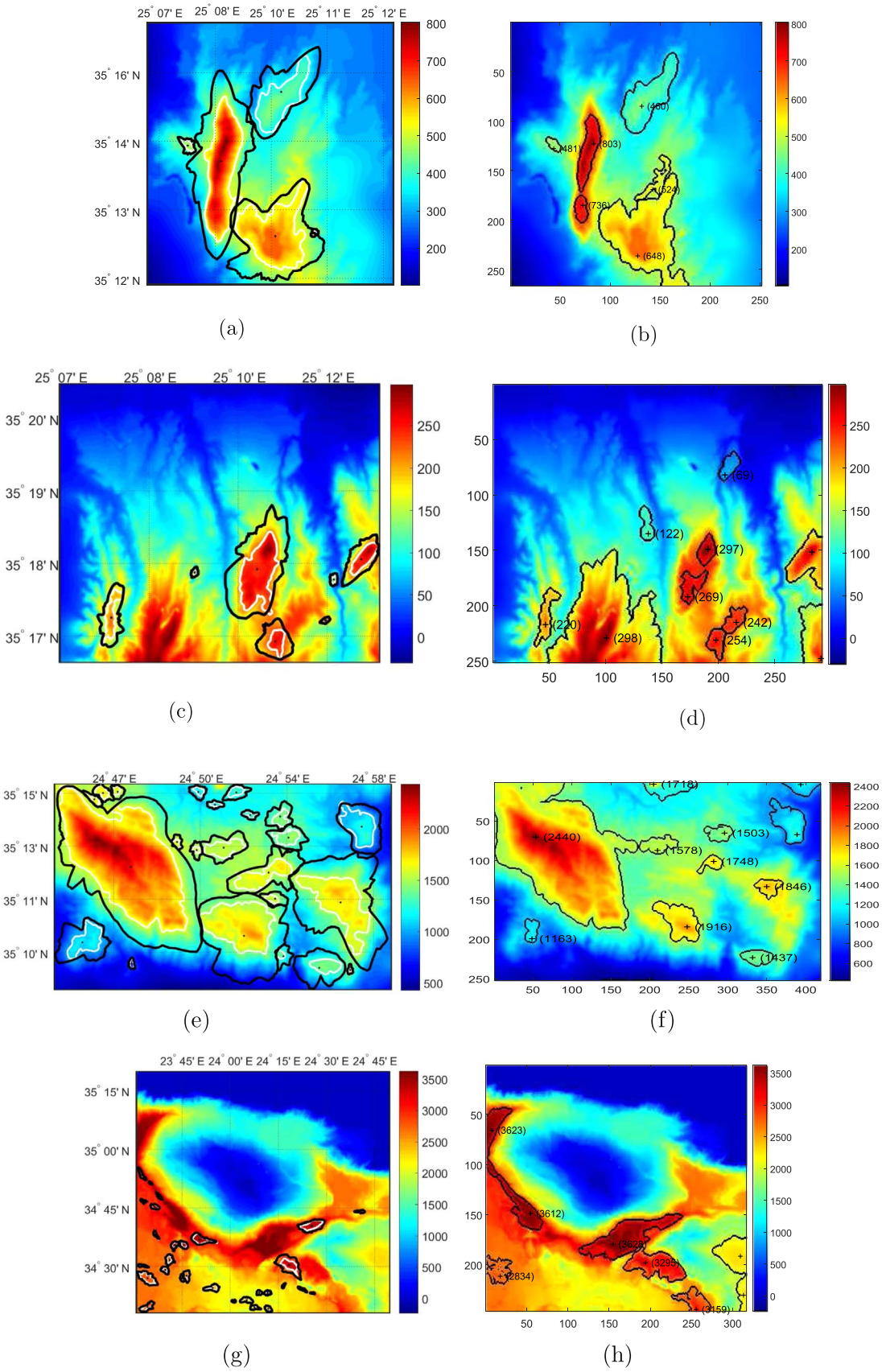

Fig. 10. Results of the MBOA method (first column) and the VOLEI method (second column) under different real DEMs. Vertical scale in (a), (b), (c) corresponds to the elevation (m) while in (d) to the sea depth (m). In the first column, the maximum altitude (m) of the detected topographic highs is given in parenthesis. WGS84 reference system has been selected for the DEMs of the MBOA method while a reference grid has been selected for indexing the DEMs of the VOLEI method.

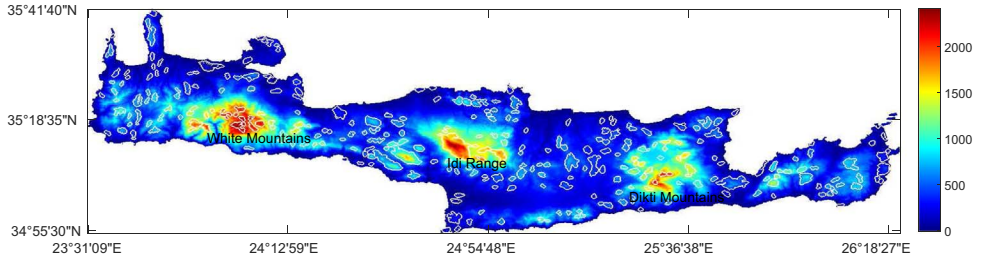

Fig. 11. Result of the VOLEI method under the Crete DEM. The vertical scale corresponds to the elevation (m). WGS84 reference system has been selected for Crete's DEM.

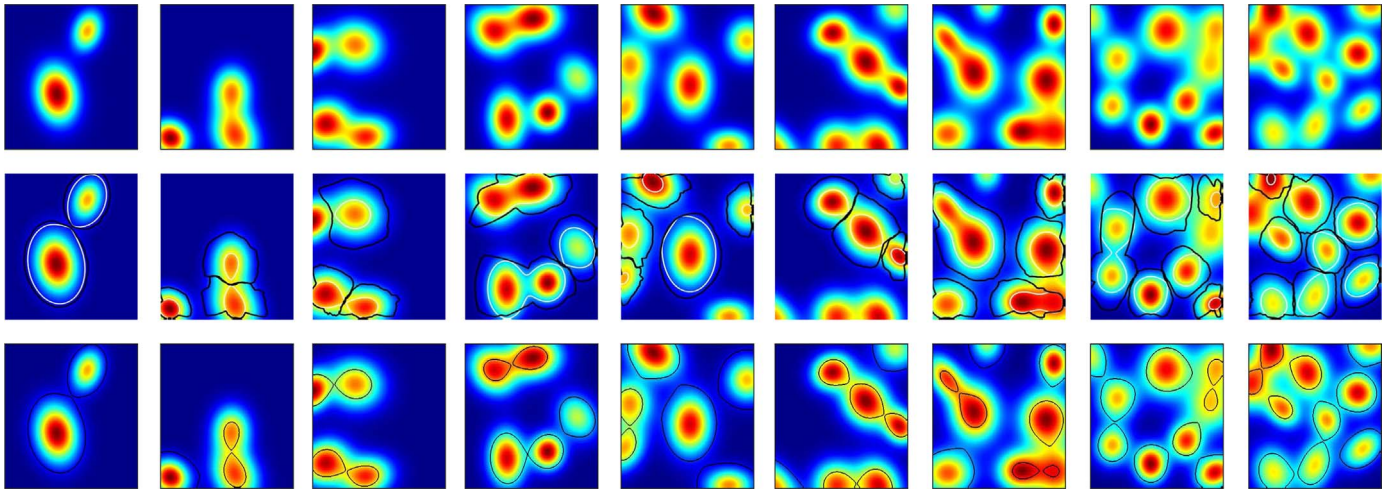

Fig. 12. First row: DEMs from synthetic dataset for different values of k. Second row: The detected highs according to MBOA method. Third row: The detected highs according to the VOLEI method.

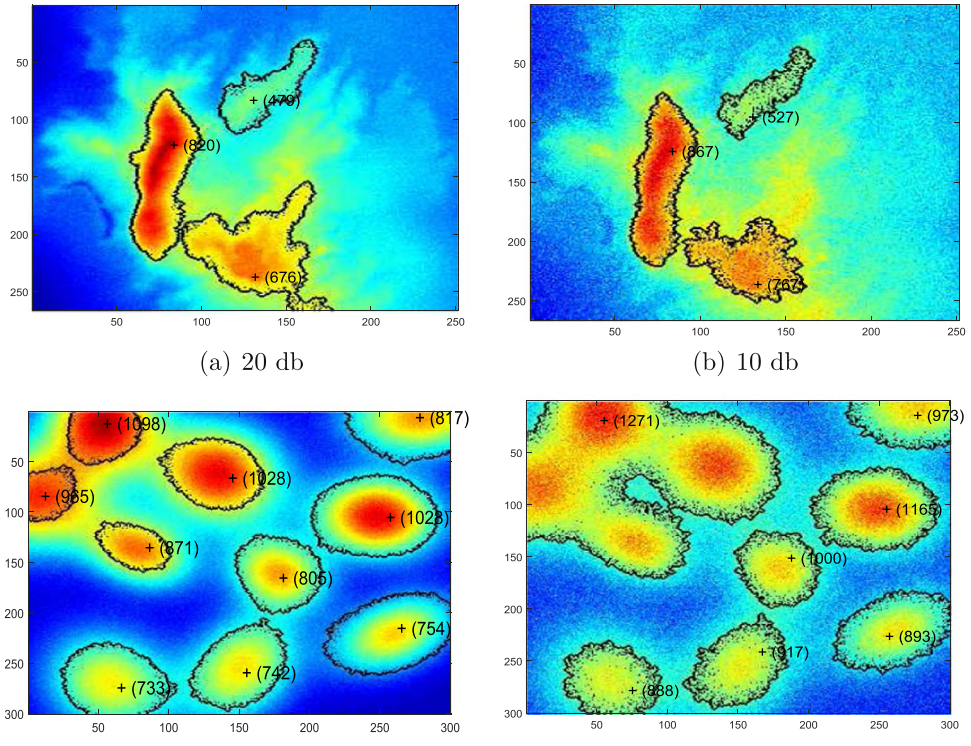

(a) 20 db (b) 10 db

(c) 20 db (d) 10 db

Fig. 13. Results of the VOLEI method under different levels of SNR on real (top) and synthetic (bottom) DEMs. A reference grid has been selecting for indexing. (a) 20 db (b) 10 db (c) 20 db (d) 10 db.

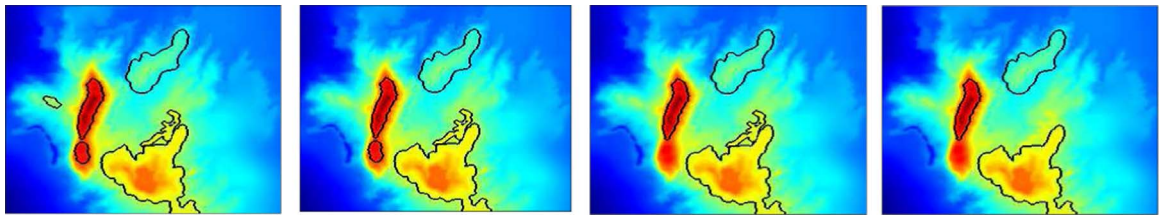

(a) $MinA = 100$ (b) $MinA = 200$ (c) $MinA = 300$ (d) $MinA = 400$

Fig. 14. High detection results of VOLEI method on Giouchtas region under different values of the parameter *MinA*. (a) *MinA*=100 (b) *MinA*=200 (c) *MinA*=300 (d) *MinA*=400.

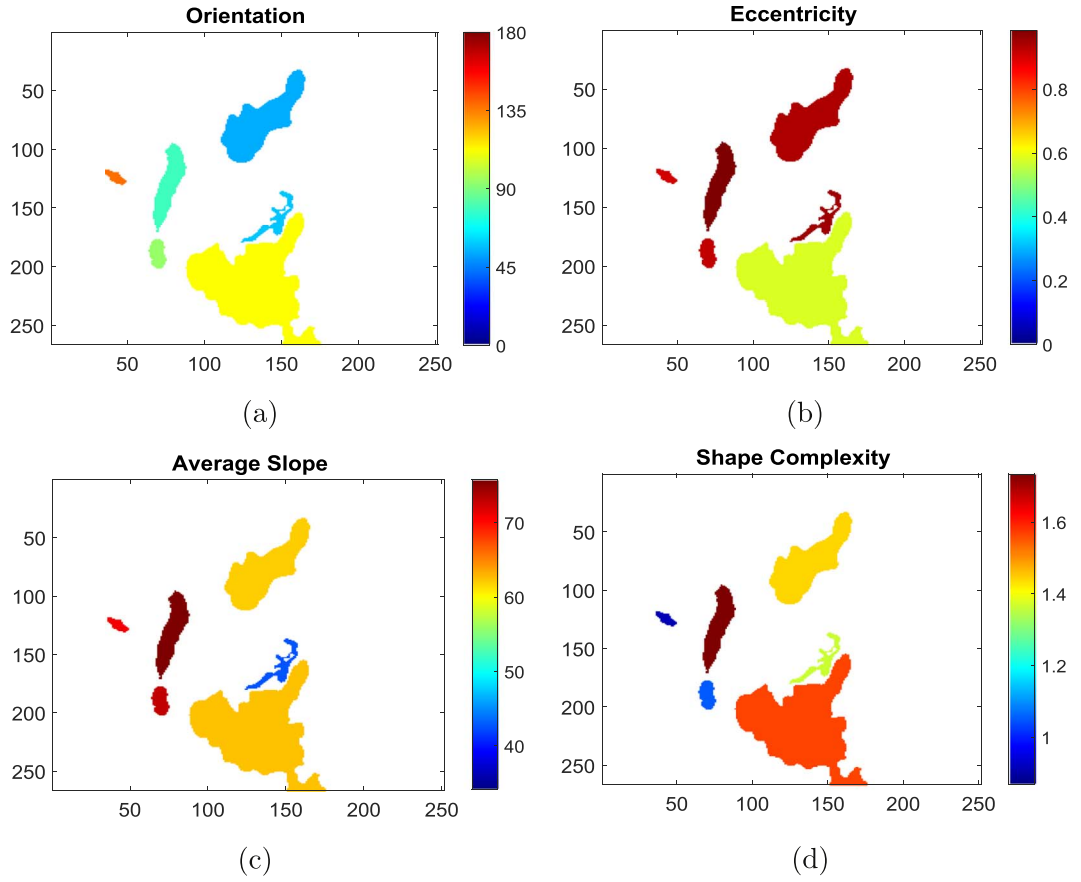

Fig. 15. The main orientation (in degrees), eccentricity, average slope (in degrees) and shape complexity of the detected highs of Giouchtas region. The orientation of zero or 180° angle is parallel on horizontal plane. A reference grid has been selecting for indexing.

$$I_{k,j}(x, y) = \sum_{i=1}^{k} G_{k,j}(x, y), \quad x, y \in \{1, \ldots, 300\} \tag{4}$$

The definition of a 2D Gaussian function $G(x, y)$ is given in the Appendix section. In order to get well discriminated highs, the minimum distance between two tops is 20% of the image diagonal. The number of the Gaussian functions k determines the number of almost elliptical shape highs on the DEM.

Fig. 12 depicts nine DEMs from the synthetic dataset for different values of k (first row), the corresponding high detections of MBOA (Bohnenstiehl et al., 2012) (second row) and the VOLEI method (third row). The isocontours (boundaries) of the detected highs are plotted with black curves (third row). It holds that under any case VOLEI method correctly detects the highs even if their tops are close together or are partly visible, while MBOA usually merges highs that are close together and fail to detect highs that are partly visible. More specifically, MBOA method provides average precision of 100% and recall of 64.6% in the detection of the highs' tops in the synthetic dataset. The VOLEI method, that clearly outperforms the MBOA method, yields 100% precision and 97.6% recall, respectively. Additionally, we have computed the average recall in detection of the highs' tops for the nine groups of different values of tops k (each group contains 20 DEMs). MBOA method yields lowest average recall 51.1% observed for k=9, while for each $k \leq 5$ it gives more than 61% average recall. The VOLEI method yields lowest average recall 93.5% observed for k=10, while for each $k \leq 5$ we get more than 99% average recall.

5.2. Robustness to noise effects

In order to evaluate the robustness of the proposed framework to noise effects, Gaussian white noise of 10 and 20 dB Signal to Noise Ratio (SNR) was added on the real DEM of Fig. 1(a) and on the synthetic DEM of Fig. 12. Especially, the case of 10 db was selected, to show the good performance of the proposed scheme on very complex DEMs. Fig. 13 depicts the isocontours (boundaries) of the detected highs with black curves. The proposed method yields high performance results on both real and synthetic data, without any false alarm, although it has not any noise removal step. In the case of 10 db, some very close highs have been merged, but the accuracy of the boundary detection remains high enough even if the resulting isocontours are

noisy.

5.3. Sensitivity analysis

This section presents the sensitivity analysis of the results concerning the user defined parameter *MinA* that determines the minimum possible expanded area of a high. Fig. 14 depicts the detected highs in Giouchtas region based on VOLEI method under different values of the parameter $MinA \in \{100, 200, 300, 400\}$. The isocontours of the detected highs are plotted with black curves. It holds that the results of the VOLEI method are not really affected by this parameter that is mainly used to ignore highs corresponding to very low areas. It holds that as the *MinA* increases, the number of detected highs decreases. For example, when *MinA* is set to 100, then six high are detected (see Fig. 14(a)), while when *MinA* is set to 400, only three highs are detected (see Fig. 14(d)).

5.4. High annotations based on geomorphological features

Digital Terrain Analysis (DTA) is the process of describing the terrain's quantitative attributes (Wilson and Bishop, 2013; Hengl et al., 2003) also referred as geomorphological analysis, landform parametrization and land surface analysis. VOLEI method provides four terrain parameters (see Section 3.3 and Fig. 15), i.e. orientation, eccentricity, average slope and shape complexity in order to quantify the morphology of a terrain. The previously mentioned terrain parameters have been selected because they are considered of great importance in earth sciences (geology, geomorphology, tectonics, hydrology, oceanography, ecology and others). Among others, these terrain parameters are used to model (Wilson and Bishop, 2013) the erosional and depositional processes, to evaluate slope hazards and wildfire propagation, to improve vegetation mapping, to predict water flow and accumulation and to study the role of surface processes on mountain evolution. For example, the shape complexity is used to describe the geometry of polygons in the sense of how oval is a detected geomorphological structure (peaks, ridges, pits, valleys). Fig. 15 depicts the main orientation (in degrees), eccentricity, average slope (in degrees) and shape complexity of the detected highs of the Giouchtas region (Kokinou et al., 2015). Prevailing orientations of the topographic highs in the study area are 55–65° (northeast-southwest) and 80–100° (almost north-south), while the eccentricity, the average slope and the shape complexity generally reveal large values probably due to the fact that this area is tectonically strongly deformed (Kokinou et al., 2015). Specifically in the work of Kokinou et al. (2015) the Giouchtas region was studied based on morphotectonic analysis in combination with detailed geological and tectonic survey. Field measurements of outcropping geological faults were used to determine the fault geometry and to reconstruct the structural development of this area. Furthermore, the geomorphic indices, used in the pre-mentioned work, i.e. the mountain front sinuosity index (Smf) and the valley floor/width ratio index (Vf) assigned this area to tectonic class I, corresponding to higher tectonic activity especially towards the north and northeast that is in agreement with the results of the geomorphological parameters revealed by the VOLEI method.

6. Conclusions

In this paper, we have proposed a framework for automatic and unsupervised detection of topographic highs. The ambiguity of the highs' boundaries is efficiently solved by suitable isocontours that are derived as solutions of a probability based optimization problem, based on the volume evolution of an isocontour starting from the top and gradually growing, as decreasing the altitude level of the isocontour. The order of the topographic high detection is given by the inclusion tree that represents the enclosure relationships among the isocontours.

The proposed approach has been evaluated on real and synthetic DEMs corresponding to the onshore (land) and offshore (sea) environment. The experimental results demonstrate the high performance of the VOLEI method on several real and synthetic topographic data and its outerperformance against MBOA method, especially under highs of complex basal shapes or partially visible in the given DEM even if they are close. This work is also considered of great importance because a formal definition of highs based on volume evolution of isocontours is proposed for the first time. The results of the proposed method can be applied in a wide range of the geoscientific disciplines such as remote sensing, topography, geology, geoarchaeology, oceanography and others. As future work we plan to apply the present methodology to enforce the detection of extensional geological faults both in direction and location, related to topographic highs and to confirm the results of the automatic detection with field measurements.

Acknowledgements

This work is partly implemented through the National Participation 2014-2016, “Reward Participation in competitive EU Programmes”, project title “NEREIDs: Embracing Innovation for Preparedness in Civil Protection & Marine Pollution, EU Humanitarian Aid and Civil Protection under Grant Agreement No. 638494/2012/ECHO/A5/SUB”. Many thanks to the anonymous reviewers and the editor for their valuable suggestions that helped us to improve this work.

Appendix

A 2D Gaussian function $G(x, y)$ of orientation θ, amplitude H, center (x_0, y_0) and spreads σ_x, σ_y is given by Eq. (8).

$$a = \frac{\cos^2(\theta)}{2\sigma_x^2} + \frac{\sin^2(\theta)}{2\sigma_y^2} \tag{5}$$

$$b = \frac{-\sin(2\theta)}{4\sigma_x^2} + \frac{\sin(2\theta)}{4\sigma_y^2} \tag{6}$$

$$c = \frac{\sin^2(\theta)}{2\sigma_x^2} + \frac{\cos^2(\theta)}{2\sigma_y^2} \tag{7}$$

$$G(x, y) = H \cdot e^{-(a(x-x_0)^2 - 2b(x-x_0)(y-y_0) + c(y-y_0)^2)} \tag{8}$$

References

Bohnenstiehl, D.R., Howell, J.K., White, S.M., Hey, R.N., 2012. A modified basal outlining algorithm for identifying topographic highs from gridded elevation data, part 1: motivation and methods. Comput. Geosci. 49, 308–314.

Booth, A.M., Roering, J.J., Perron, J.T., 2009. Automated landslide mapping using spectral analysis and high-resolution topographic data: puget sound Lowlands, Washington, and Portland hills, Oregon. Geomorphology 109, 132–147.

Cavalli, M., Marchi, L., 2008. Characterisation of the surface morphology of an alpine alluvial fan using airborne lidar. Nat. Hazards Earth Syst. Sci. 8, 323–333.

Davis, P.A., 2012. Airborne digital-image data for monitoring the Colorado River corridor below Glen Canyon Dam, Arizona, 2009-Image-mosaic production and comparison with 2002 and 2005 image mosaics. Technical Report. US Geological Survey.

Dinesh, S., 2006. Extraction of mountains from digital elevation models using mathematical morphology. GIS Dev. Malays. 1, 16–19.

Drăguţ, L., Blaschke, T., 2006. Automated classification of landform elements using object-based image analysis. Geomorphology 81, 330–344.

Euillades, L.D., Grosse, P., Euillades, P.A., 2013. Netvolc: an algorithm for automatic delimitation of volcano edifice boundaries using dems. Comput. Geosci. 56, 151–160.

Frankel, K.L., Dolan, J.F., 2007. Characterizing arid region alluvial fan surface roughness with airborne laser swath mapping digital topographic data. J. Geophys. Res.: Earth Surf., 112.

Hengl, T., Gruber, S., Shrestha, D., 2003. Digital Terrain Analysis in ILWIS. International Institute for Geo-Information Science and Earth Observation Enschede, The Netherlands, 62.

Hong, B.W., Sohn, B.S., 2010. Segmentation of regions of interest in mammograms in a topographic approach. IEEE Trans. Inf. Technol. Biomed. 14, 129–139.

Iwahashi, J., Pike, R.J., 2007. Automated classifications of topography from dems by an unsupervised nested-means algorithm and a three-part geometric signature. Geomorphology 86, 409–440.

Kokinou, E., Skilodimou, H., Bathrellos, G., Antonarakou, A., Kamberis, E., 2015. Morphotectonic analysis, structural evolution/pattern of a contractional ridge: Giouchtas mt., Central Crete, Greece. J. Earth Syst. Sci. 124, 587–602.

Kweon, I.S., Kanade, T., 1994. Extracting topographic terrain features from elevation maps. CVGIP: Image Underst. 59, 171–182.

Micheal, A.A., Vani, K., 2015. Automatic mountain detection in lunar images using texture of dtm data. Comput. Geosci. 82, 130–138.

Miliaresis, G.C., Argialas, D., 1999. Segmentation of physiographic features from the global digital elevation model/gtopo30. Comput. Geosci. 25, 715–728.

Obu, J., Podobnikar, T., 2013. Algorithm for karst depression recognition using digital terrain models. Geod. Vestn. 57, 260–270.

Panagiotakis, C., Grinias, I., Tziritas, G., 2011. Natural image segmentation based on tree equipartition, bayesian flooding and region merging. IEEE Trans. Image Process. 20, 2276–2287.

Panagiotakis, C., Kokinou, E., 2014. Automatic enhancement and detection of active sea faults from bathymetry. In: International Conference on Pattern Recognition (ICPR). pp. 855–860.

Panagiotakis, C., Kokinou, E., 2015. Linear pattern detection of geological faults via a topology and shape optimization method. IEEE J. Sel. Top. Appl. Earth Obs. Remote Sens. 8, 3–11.

Panagiotakis, C., Ramasso, E., Tziritas, G., Rombaut, M., Pellerin, D., 2008. Shape-based individual/group detection for sport videos categorization. Int. J. Pattern Recognit. Artif. Intell. 22, 1187–1213.

Podobnikar, T., 2012. Detecting mountain peaks and delineating their shapes using digital elevation models, remote sensing and geographic information systems using autometric methodological procedures. Remote Sens. 4, 784–809.

Slatton, K.C., Carter, W.E., Shrestha, R.L., Dietrich, W., 2007. Airborne laser swath mapping: achieving the resolution and accuracy required for geosurficial research. Geophys. Res. Lett., 34.

Smith, M., Rose, J., Booth, S., 2006. Geomorphological mapping of glacial landforms from remotely sensed data: an evaluation of the principal data sources and an assessment of their quality. Geomorphology 76, 148–165.

Tarolli, P., Arrowsmith, J.R., Vivoni, E.R., 2009. Understanding earth surface processes from remotely sensed digital terrain models. Geomorphology 113, 1–3.

Wilson, J., Bishop, M., 2013. Geomorphometry. J. Shroder (editor in chief), MP Bishop (Ed.), Treatise on Geomorphology 3, 162–186.